Proceedings of the 21st ICSMGE, Vienna, Austria, 14 – 19 June 2026. Pistrol, Adam & Schweiger (eds.)
Published by: ÖGG, Austrian Society for Geomechanics, Salzburg, Austria, ISBN 978-3-9503898-4-5
https://doi.org/10.53243/ICSMGE2026-409

Theoretical and numerical evaluation of tunnel-soil system stability using the second-order work criterion

Ebtehal Hameed, Florent Prunier
Université de Lyon, INSA de Lyon, GEOMAS, France, ebtehal.hameed@insa-lyon.fr

ABSTRACT: In this paper, a comprehensive numerical and theoretical analysis of the stability of tunnel-soil systems has been carried out through the second-order work criterion. The aim is to identify at both the local and global level instabilities in stratified grounds around tunnels under the effect of a mechanical action. In order to simulate a realistic construction environment, a two-dimensional FEM model was developed by MATLAB, which employed strain-softening behavior and staged excavation. The model outputs include displacement fields, stress redistribution, plastic strain, and the normalised shear stress. The second-order work condition is used in the post-processing to detect when the early stages of instability occur before more traditional failure limits are reached. It is found that localized zones of energy dissipation can be an indicator of instability, and it is a useful tool for assessing tunnel safety at design. This approach creates a reliable structure for evaluation of tunnel safety without requiring the use of field data, and it highlights the possibility of using second-order work as a predictive index in numerical soil mechanics applications.

KEYWORDS: Second-order work criterion, numerical modeling, soil stability.

1 INTRODUCTION

The stability of tunnel-soil systems is widely regarded as a priority problem in geotechnical engineering, particularly in stratified soil layers and in urban areas with a high concentration of structures. Material strength at failure can be assessed using traditional failure criteria, such as the Mohr-Coulomb criterion. However, such models may concern only peak strength and may not fully represent the mechanisms leading up to the onset of failure, particularly for complex loadings or for loose to moderately consolidated soil (Nova, 1994; Darve and Laouafa, 2000; Labuz and Zang, 2015).

To overcome these drawbacks, energy criteria have been established to provide a more holistic approach to stability assessment. In geomaterials, instability reflects different physical mechanisms depending on the material type. In soils, instability generally corresponds to a progressive loss of stiffness or strength, leading to strain localization or static liquefaction as deformation accumulates. In contrast, in rocks, it is typically associated with brittle failure or rock burst, characterized by the sudden release of stored elastic energy and rapid collapse.

The second-order work criteria consider the sign of the scalar product between incremental stress and strain. Early notions of (Hill, 1958) presented that such a scalar product, it is provides a unified energetic framework capable of identifying both behaviors by detecting the transition from stable positive incremental work to unstable zero or negative incremental work. mechanical response due to lessened stiffness and energy absorption capacity even before failure indicators show visibly (Darve et al., 2004; Nicot and Darve, 2007).

The concept has been developed in numerical modeling and finite element contexts to calculate second-order work locally at material points or globally at the boundaries of the structure (Prunier et al., 2009; Nicot and Darve, 2011).

Many studies showed its value in identifying instability across a variety of geomechanical problems, including tunnel collapse, static liquefaction, and shear band development (Prunier et al., 2016; Zeng et al., 2019).

Despite its strong theoretical foundation, the second-order work criterion remains underutilized in tunnel–soil interaction studies, particularly for early excavation stages where instability often initiates. The study tackles this gap by modelling the excavation of a tunnel in a stratified geological profile through a MATLAB-based finite element approach. Using the Croix-Rousse tunnel as a reference case, the analysis combines local and global forms of the second-order work criterion to identify when and where instability begins to develop. This provides a practical way to anticipate stability issues during the design phase of tunnel projects.

2 THEORETICAL BACKGROUND

Hill (1958) showed that a deformable body remains mechanically stable only when the incremental internal work associated with any admissible virtual displacement field δu is strictly positive. This requirement is expressed in Equation (1):

$$\int_V \delta\sigma_{ij}\, \delta\left(\frac{\partial u_i}{\partial X_j}\right) dVo > 0 \qquad (1)$$

In this relation, $\delta\sigma_{ij}$ is the increment of the nominal stress, while $\delta(\partial u_i/\partial X_j)$ represents the incremental change in the displacement gradient. Both quantities are defined with respect to the material coordinates X_j and evaluated over the undeformed reference domain Vo. The term dVo denotes an infinitesimal volume element used to integrate the incremental internal work.

A strictly positive value of the integral means that additional external work is needed for deformation to continue, indicating that the system is stable. If the integral becomes zero or negative, deformation can proceed without further external energy, signalling the onset of instability.

As this principle was further explored and applied in numerical and constitutive modeling, particularly under small-strain and small-displacement assumptions, it has allowed this principle to be expressed in a simplified form known as the second-order work criterion.

This concept has evolved into two main forms: a local formulation and a global formulation, each offering distinct insights into system stability.

2.1 *Local second-order work criterion*

The local second-order work w_2 assesses stability at the material-point scale, commonly at Gauss integration points in finite element analyses. It quantifies whether a small incremental disturbance at a given location results in a release or a demand for energy. In doing so, it highlights zones where the material response begins to soften, allowing early detection of localized instability. The local second-order work is defined in Equation (2):

$$w_2 = \delta\sigma : \delta\varepsilon \qquad (2)$$

Where δσ is the stress increment, and δε is the corresponding strain increment. Under finite element discretization strain increment is obtained from Equation (3):

$$\delta\varepsilon = B \cdot \delta Qe \tag{3}$$

Where B is the strain-displacement matrix, and δQe is the nodal displacement increment of the element. The stress increment is computed from the constitutive law according to Equation (4):

$$\delta\sigma = D.\delta\varepsilon \tag{4}$$

where D is the elastic-plastic tangent stiffness matrix, a loss of material stability, typically associated with the onset of strain localization or the formation of shear bands, as reported by (Darve and Laouafa, 2000; Hadda et al., 2013).

2.2 *Global second-order work criterion*

The global second-order work W_2 provides an overall measure of stability by evaluating how much energy the system exchanges during a small loading increment. In finite element analysis, it reflects the balance between the internal force increments and the associated displacement increments across the whole domain, offering a macroscopic perspective on the system's stability.

The theoretical expression of global second-order work is defined as Equation (5):

$$W_2 = \int_V \delta\sigma : \delta\varepsilon \, dV \tag{5}$$

In a finite element setting, this can be equivalently computed from nodal quantities as Equation (6):

$$W_2 = \delta U^t \cdot \delta F \tag{6}$$

Where δU is the vector of incremental nodal displacements, and δF is the corresponding vector of incremental nodal forces. When W_2 drops significantly, particularly as it approaches zero, it indicates that the structure is losing its ability to absorb or dissipate energy, signalling the approach of a global instability.

This indicator has been widely adopted in geotechnical engineering and has shown strong relevance for tunnel stability assessment, where complex loading and boundary conditions make conventional criteria less reliable (Nicot and Darve, 2007; Prunier et al., 2016; Zhang et al., 2021).

3 NUMERICAL MODELING APPROACH

A special validation process was used to confirm that the second-order work criterion for tunnel stability assessment was applied correctly. This process creates a clear link between the criterion's numerical formulation and theoretical definition.

The indication was integrated into a MATLAB finite element code created at the GEOMAS Laboratory. The Croix-Rousse tunnel's staged excavation was numerically simulated for validation. The analysis focused on the local and global aspects of second-order work.

3.1 *Constitutive model*

To capture the progressive degradation of the mechanical strength of the soil surrounding the tunnel during excavation, a strain-dependent constitutive model was adopted. The model incorporates both hardening and softening mechanisms by allowing the friction angle and cohesion to evolve as functions of the equivalent plastic strain, denoted as ε^p_{eq}. This internal variable is defined using the deviatoric plastic strain tensor ε^p as explained in Equation (7):

$$\varepsilon^p_{eq} = \sqrt{\frac{2}{3} tr(\varepsilon^p - \frac{tr(\varepsilon^p)}{tr} I)^2} \tag{7}$$

The friction angle and cohesion evolve according to the following hardening and softening laws, as shown in Equation (8) and Equation (9), respectively:

$$\phi = \phi_0 + \frac{(\phi_f - \phi_0)\varepsilon^p_{eq}}{B_p + \varepsilon^p_{eq}} \tag{8}$$

$$c = c_0 + \frac{(c_f - c_0)\varepsilon^p_{eq}}{B_c + \varepsilon^p_{eq}} \tag{9}$$

Here, ϕ_0 and c_0 are the initial friction angle and cohesion, while ϕ_f and c_f represent their respective asymptotic values at large strains. The parameters B_p and B_c represent the equivalent plastic strain levels at which the friction angle and cohesion, respectively, reach 50% of their transition between the initial and residual values. The Croix-Rousse tunnel's known site characteristics were used to determine these parameters, which are presented in Table 1.

3.2 *Material and Soil Properties*

The numerical model incorporates the heterogeneous geological conditions observed along the tunnel alignment, which is characterized by three principal layers: Pliocene clays, Miocene marls, and a weathered granite bedrock.

The tunnel is entirely embedded within the Miocene marl, the second layer, a relatively soft sedimentary unit composed of fine calcareous sandy marls with a silty matrix. This formation exhibits intermediate mechanical behavior, lying between that of cohesive soils and weak rocks, characterized by moderate stiffness and a tendency to strain-softening under unloading. The Miocene layer governs most of the deformation and energy dissipation during excavation due to its low strength and progressive degradation of stiffness (Grand Lyon & EGIS Tunnels, 2010).

According to the Croix-Rousse Geotechnical and Hydrogeological Report (Grand Lyon & EGIS Tunnels, 2010), three aquifers are present within the hill, but the deep molasse aquifer is efficiently drained by existing tubes and galleries. The measured water levels (162–167 m NGF) are well below the tunnel axis (175–190 m NGF). Consequently, the model assumes dry conditions, and all computed stresses correspond to effective stresses equal to total stresses.

The mechanical parameters of each layer were derived from the same report and are summarized in Table 1.

Table 1. Soil layer properties.

Parameter	Symbol	Granite	Miocene	Pliocene
Density (kg/m³)	ρ	2600	2000	1900
Young's modulus (MPa)	E	1000	204	28
Poisson's ratio	ν	0.3	0.3	0.3
Dilation angle (∘)	ψ	5	3	0
Cohesion (kPa)	$c_f = c_0$	250	20	10
Friction angle (∘)	ϕ_f	45	35	30
Initial friction angle (∘)	ϕ_0	1	1	5
Plastic strain parameter	B_p	0.0003	0.0003	0.0007

In Phase 3, the structural support of the tunnel was represented by an elastic HEB-type steel beam applied along the excavation

boundary. The equivalent mechanical properties are summarized in Table 2.

Table 2. Equivalent properties of the tunnel support (HEB beam).

Properties	HEB beam
Young's modulus (MPa)	210000
Cross-sectional area (cm^2)	91*α
Second moment of area (cm^4)	8091*α
Spacing coefficient (2m spacing between elements)	0.5

3.3 *Finite element model implementation*

To evaluate the stability of the tunnel–soil system during staged excavation, a custom finite element code was developed in MATLAB, modeled as a 2D plane strain problem using triangular linear elements as shown in Figure 1.

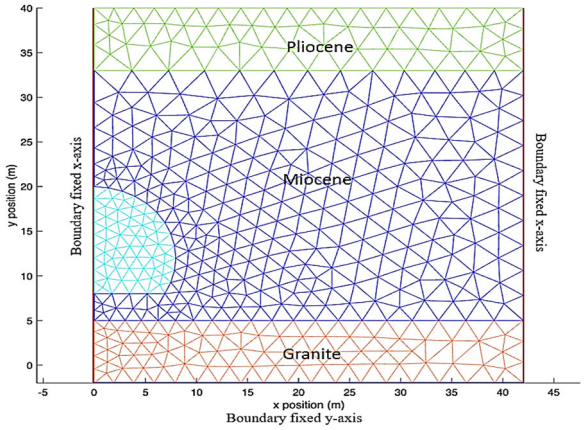

Figure 1. Finite element mesh and boundary conditions.

Boundary conditions were applied to reflect realistic in-situ stress conditions. Vertical displacements are fixed at the base of the model, and horizontal displacements are restricted on both lateral edges. During the excavation sequence, constraints are imposed along the tunnel boundary to simulate support conditions at each step.

The initial stress field in Phase 1 was generated automatically through gravity loading rather than by prescribing constant K_0 values. This procedure allows each geological layer to reach equilibrium based on its own stiffness and Poisson's ratio, resulting in realistic horizontal stress variations with depth. Small plastic strains developed during initialization, removing the need for explicitly defined K_0 values.

The simulation was structured into three phases to replicate excavation and structural support installation. The total computation time for the full sequence was about 5 minutes. These are summarized in Table 3.

Table 3. Excavation phases and boundary conditions.

Phase	Loading type	Boundary conditions
Phase 1	Gravity loading and overloading at the tunnel crown.	Fixed displacements at base and lateral sides; kinematic constraints along the tunnel boundary.
Phase 2	Partial unloading 50% reduction in confinement.	unloading applied on the tunnel interface to simulate a 50% reduction in support pressure; base remains fixed.
Phase 3	Beam support insertion and complete unloading 100%.	Activate the support domain and apply interface constraints. Simulate the rest of the reduction support pressure100%.

Our numerical model is based on the convergence–confinement method (Panet et al., 2001), where the deconfinement rate λ aims to simulate the 3D excavation process by introducing a fictive radial pressure that initially balances the geostatic pressure at the boundary of the tunnel, and that is progressively released due to tunnel advance in a 2D simulation framework. The relationship between λ and the tunnel-face distance d is expressed as Equation (10)(Panet et al., 2001):

$$\lambda_d = 1 - 0.75\left[\frac{0.75R}{0.75R + d}\right]^2 \quad (10)$$

when assuming an elastic regime for the soil mass and a circular tunnel.

In the present simulation, Phase 2 represents a partially unsupported stage with d≈1 m (corresponding to λ=50%when assuming an elastic regime and a circular tunnel), while Phase 3 corresponds to complete deconfinement of the soil mass λ=100% and activation of the beam support, representing a large tunnel-face distance where the section is fully excavated and structurally supported.

4 RESULTS AND DISCUSSION

4.1 *Deformation response of soil domain*

The deformation mesh shown in Figure 2 corresponds to the cumulative displacement field between the end of Phase 1 (initial geostatic equilibrium) and the end of Phase 3 (post-excavation with support installation). Displacements are magnified by a factor of 10 for visualization clarity.

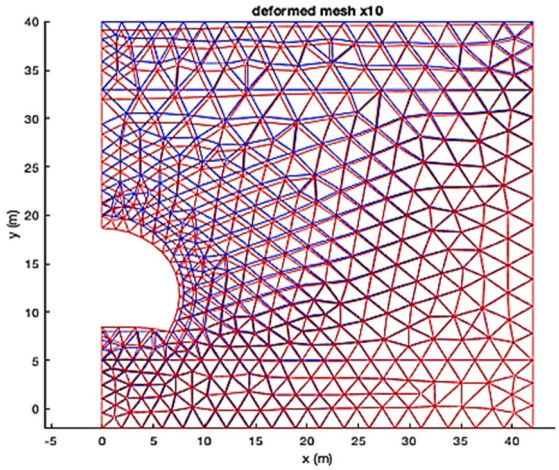

Figure 2. The deformed mesh of the tunnel model.

Displacements are clearly concentrated near the tunnel crown and invert, where the loss of confinement has the greatest impact. The softer surrounding layers, particularly the Miocene and Pliocene, show more pronounced deformation compared to the stiffer granite base, consistent with their lower elastic moduli.

This distribution of deformation is expected and aligns well with what has been reported in prior numerical and analytical studies on tunnel excavation (Loganathan and Poulos, 1998; Oreste, 2003)

In our case, the observed displacement gradients also correlate with zones where local second-order work began to decline, indicating early signs of instability. This will be discussed further about second-order work results in the following figures.

4.2 *Stress redistribution around the tunnel*

After tunnel excavation, the numerical simulation shows a significant redistribution of vertical σy and horizontal σx stresses. These findings are consistent with Phase 3, which is the state following complete excavation and beam support activation.

Horizontal stresses show a marked decrease at the tunnel invert and springlines, as shown in Figure 3, and a significant rise at the crown, where values reach about 300 kPa.

This stress distribution is consistent with the typical arching effect, in which the excavation process causes a load transfer away from the hole and toward more stable surrounding parts, particularly the crown. This behavior is consistent with Vermeer's previous studies, which revealed comparable arching paths under deformation-controlled tunneling settings (Vermeer et al., 2002).

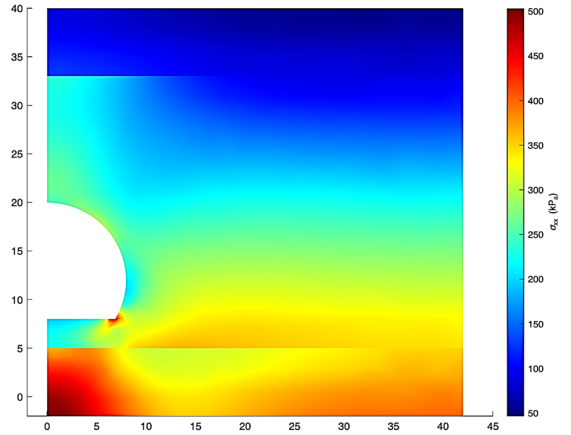

Figure 3. Horizontal stress distribution after excavation.

On the other hand, as Figure 4 illustrates, the vertical stress field exhibits an inverse distribution, with higher concentrations throughout the tunnel at the springlines and stress relief at both the crown and invert.

Peak vertical stresses in these zones surpass 900 kPa, consistent with the load redistribution mechanisms described in the convergence confinement method (Panet, 1995).

This stress transfer migrating from the roof toward the springlines reflects the arching-related confinement loss and has been analytically verified through ground reaction curve models (Vlachopoulos and Diederichs, 2009).

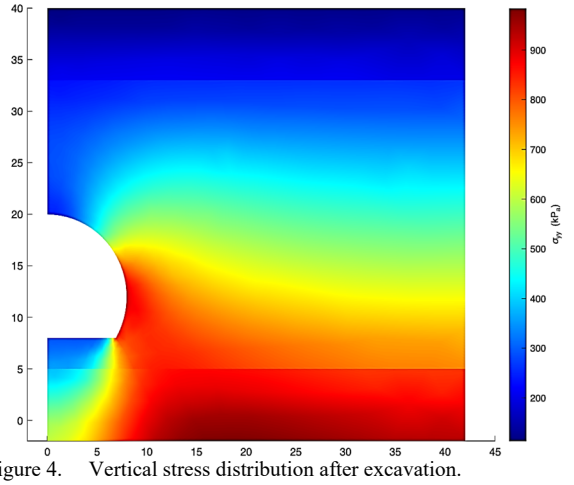

Figure 4. Vertical stress distribution after excavation.

This redistribution of stress validates the mechanical consistency of the numerical model. It forms the basis for subsequent analysis of plastic deformation and second-order work indicators.

4.3 *Distribution of normalized shear stress*

To characterize the stress state evolution during tunnel excavation, the mobilized shear stress ratio τ_{rel} is used. It quantifies the degree of shear mobilization relative to the maximum possible state under the same mean stress and is defined as Equation (11):

$$\tau_{rel} = \sqrt{\frac{J_2}{J_{2\,max}}} \tag{11}$$

Where J_2 is the second invariant of the deviatoric stress tensor S, and tr (·) denotes the trace operator (sum of the diagonal components) as explained in Equation (12):

$$J_2 = \frac{1}{2} tr(S \cdot S) \tag{12}$$

A value of $\tau_{rel} \approx 1$ indicates that the material has fully mobilized of shear strength, suggesting imminent yielding or failure, whereas lower values correspond to elastic or partially mobilized states. The normalized shear stress ratio shows a clear concentration of high values along the tunnel invert and springline, indicating zones of intense shear mobilization and potential local instability.

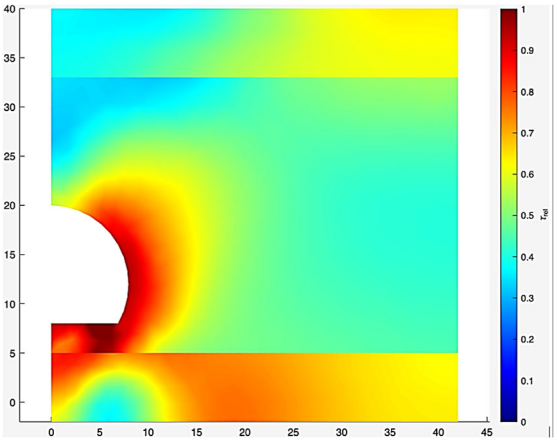

Figure 5. Normalized shear stress around the tunnel after excavation.

Figure 5 illustrates the normalized shear stress, and it can see how zones with τ_{rel} >0.8 closely match areas with negative second-order work. This correlation shows that the high shear mobilization, which reflects a decrease in the material's ability to disperse energy, is closely associated with the beginning of instability.

Shear mismatch and localized plasticity are indicated by elevated τ_{rel} values, which usually occur close to the interfaces between stiff and soft strata. Therefore, keeping an eye on τ_{rel} while excavating allows for the early identification of possible failure zones. It provides an efficient way to forecast both local and global instability mechanisms

4.4 *Distribution of equivalent plastic strain*

The distribution of equivalent plastic strain ε_{eq}^{p} identifies zones of irreversible deformation induced by excavation. As shown in Figure 6, high strain values are concentrated near the tunnel invert and sidewalls within the Miocene layer, reflecting confinement loss and stress redistribution. Peak exceeds 1.4%, marking active yielding and softening zones, particularly in the weaker Miocene and Pliocene strata compared to the stiffer granite base.

The localized plastic strain zones ccorresponds closely to areas of high mobilized shear stress, confirming their role as early indicators of instability. This correlation validates the model's robustness and agrees with prior studies (Zhang et al.,

2021; Qi et al., 2025) showing that strain localization precedes global failure. Monitoring plastic strain during excavation provides a practical means for early detection of potential failure zones in stratified or weak formations.

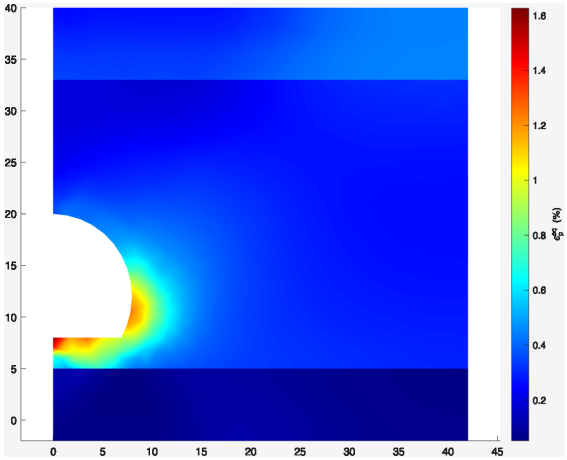

Figure 6. Equivalent plastic strain around the tunnel after excavation.

4.5 *Local second-order work*

Besides validating classical geomechanical behavior, the results obtained in this study confirm the practical usefulness of the second-order work criterion in identifying the early stages of instability. As shown in Figure 7, negative w_2 values develop predominantly along the tunnel invert, indicating local loss of stiffness and internal resistance caused by excavation-induced stress redistribution. Values approaching zero are also observed along the tunnel springlines, marking the onset of energy dissipation and progressive instability.

Similar localized deformation and failure evolution were also observed by (Zhang et al., 2021), who used discrete element simulations to analyze the stability of a shallow shield tunnel in silty fine sand. Their results showed that energy dissipation and shear strain accumulation progressively enlarged the failure zone ahead of the tunnel face, confirming that instability initiation is governed by localized mechanical degradation rather than sudden collapse.

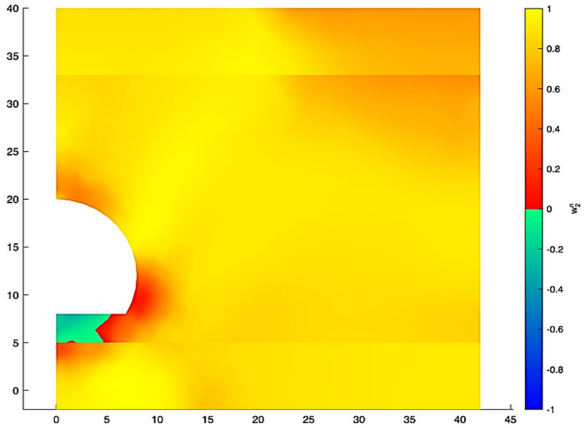

Figure 7. Local second-order work distribution w_2 around the tunnel boundary.

Although negative values of w_2 are observed at the tunnel invert, they mainly indicate the onset of local instability rather than a fully developed collapse. The model captures incipient zones of energy loss.

A complete collapse mechanism would require continuing the analysis beyond the stability limit using large-strain or dynamic numerical formulations to reproduce the full evolution of shear band propagation and ground settlement. The numerical FEM code is written in a standard quasi-static framework and assumes small small-strain assumption. As a consequence, this tool is not able to capture the global collapse mechanism.

Reproducing such phenomena would require advanced large-strain or dynamic formulations. Within this framework, w_2 remains a valuable energetic indicator, capable of detecting the transition from stable to unstable mechanical response before visible failure occurs.

The second-order work, integrated over the entire soil mass, can be robustly evaluated by measuring the incremental reaction forces and displacements at the soil–support interface, providing a practical means of assessing system stability in both experimental and numerical contexts.

4.6 *Evolution of normalized second-order work with excavation progress*

To investigate the onset of global instability during tunnel excavation, the normalized global second-order work W_2^n is employed as an energy-based stability indicator. This parameter reflects the balance between incremental internal and external work during each loading step, offering a thermodynamically consistent measure of material degradation and imminent failure as explained in Equation (13):

$$W_2^n = \frac{\delta U^t . \delta F}{\int_V \| \delta\sigma \| . \| \delta\varepsilon \| \, dV} \tag{13}$$

where δU and δF are the incremental nodal displacement and reaction force vectors at the soil–support interface, respectively; $\delta\sigma$ and $\delta\varepsilon$ denote the incremental stress and strain tensors within the domain V, and the denominator serves as a normalization factor to render W_2^n dimensionless and bounded between -1 and +1.

Figure 8 shows the evolution of normalized second-order work criteria as a function of the confinement release rate λ for both free and retained unloading paths. The results indicate that W_2^n remains nearly constant and close to 1 up to approximately λ=70%, corresponding to a stable regime with adequate energy dissipation capacity. Beyond this threshold, a pronounced decrease in W_2^n is observed, signifying a rapid reduction in global stiffness and the onset of unstable behavior. This turning point marks the transition from a stable to an unstable excavation stage, where the system can no longer absorb deformation energy effectively.

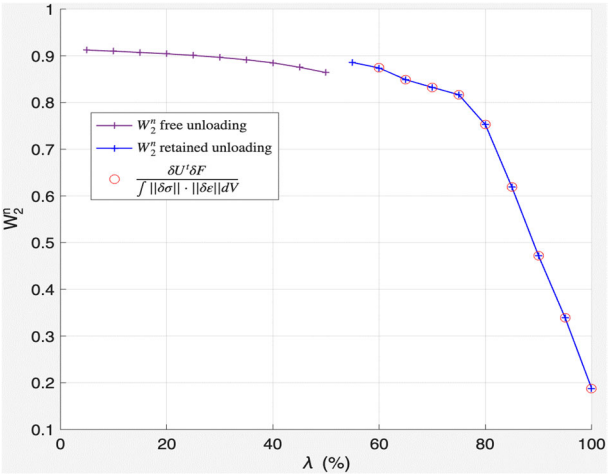

Figure 8. Evolution of Normalized Global Second-Order Work W_2^n versus Confinement Release Rate λ.

It is necessary to distinguish the two indicators more clearly. By integrating across the whole finite-element mesh, the normalized global second-order work W_2^n is derived, which represents the overall evolution of energy inside the soil mass. The incremental nodal quantities $\delta U.\delta F$, on the other hand, are exclusively calculated along the tunnel boundary, where the earth directly interacts with the structural support. Rather than describing the behaviour of the full domain, this boundary quantity captures the incremental energy exchanged at the soil–support interface.

The numerical results highlight the usefulness of the second-order work criterion as a stability indicator. Its sensitivity to confinement loss and stiffness degradation allows it to signal the onset of failure at an early stage. When the global measure W_2^n is interpreted together with local indicators, such as zones of plastic strain accumulation or areas where the mobilized shear stress becomes high, the overall ability to identify both localized and system-wide instabilities during staged excavation is significantly improved.

5 CONCLUSIONS

The second-order work criterion provides an energy-based method to evaluate the beginning of instability prior to obvious failure. By detecting the loss of stiffness and energy dissipation capacity, it enhances traditional techniques and offers a more accurate and timely failure warning. It is an effective diagnostic and design tool for practitioners, particularly in complicated ground conditions. Its incorporation into numerical modeling and monitoring systems in the future may improve the assessment of stability in geotechnical engineering practice.

The primary outcome of this work is the proof that the incremental nodal reaction forces and displacements at the interface between the soil and its support are sufficient to precisely calculate the integral of the local second-order work across the entire soil volume. The monitoring of the stability of the entire ground mass during tunneling operations would therefore be substantially improved by giving special focus to the development of measurement techniques for these variables.

The numerical analyses replicated common mechanisms of stress redistribution surrounding the tunnel, such as the arching effect and stress development along the invert and springlines. The patterns of plastic strain and mobilized shear stress aligned with typical zones of progressive failure within the softer geological layers. When interpreted together, the local and global forms of the second-order work criterion provided a coherent picture of how instability initiates and develops:

1. The local second-order work analysis revealed the onset of instability along the tunnel boundary, particularly at the invert and springlines. These areas exhibited pronounced plastic strain localization together with high levels of mobilized shear stress ($\tau_{rel} > 0.8$), indicating that the loss of incremental energy is closely associated with the initiation of failure
2. The normalized global second-order work W_2^nproved to be a robust macroscopic indicator of system stability. A marked drop in W_2^n was observed once the confinement release approached roughly 70%, signalling a clear transition from stable behaviour to an unstable phase of the excavation.
3. The findings indicate that only the incremental reaction forces and displacements at the soil–support interface may be used to reliably calculate the integral of local second-order work over the entire soil domain, offering a useful method for monitoring global stability.
4. The ability to identify both local and global instabilities is improved by incorporating second-order work indicators into numerical and monitoring frameworks. In complicated, nonlinear, and stratified geological formations, this method holds great promise for real-time stability assessment and tunnel design optimization.

6 REFERENCES

Darve, F. and Laouafa, F., 2000. Instabilities in granular materials and application to landslides. *Mechanics of Cohesive-frictional Materials*, 5(8), pp.627–652.

Darve, F., Servant, G., Laouafa, F. and Khoa, H.D.V., 2004. Failure in geomaterials: continuous and discrete analyses. *Computer Methods in Applied Mechanics and Engineering*, 193(27), pp.3057–3085.

Grand Lyon & EGIS Tunnels, 2010. *Tunnel – Mémoire géologique, géotechnique et hydrogéologique*. Lyon, France (unpublished).

Hadda, N., Nicot, F., Bourrier, F., Sibille, L., Radjai, F. and Darve, F., 2013. Micromechanical analysis of second order work in granular media. *Granular Matter*, 15(2), pp.221–235.

Hill, R., 1958. A general theory of uniqueness and stability in elastic-plastic solids. *Journal of the Mechanics and Physics of Solids*, 6(3), pp.236–249.

Labuz, J.F. and Zang, A., 2015. Mohr–Coulomb Failure Criterion. In: R. Ulusay, ed. *The ISRM Suggested Methods for Rock Characterization, Testing and Monitoring: 2007-2014*. [online] Cham: Springer International Publishing. pp.227–231.

Loganathan, N. and Poulos, H.G., 1998. Analytical prediction for tunneling-induced ground movements in clays. *Journal of Geotechnical and geoenvironmental engineering*, 124(9), pp.846–856.

Nicot, F. and Darve, F., 2007. A micro-mechanical investigation of bifurcation in granular materials. *International Journal of Solids and Structures*, 44(20), pp.6630–6652.

Nicot, F. and Darve, F., 2011. Diffuse and localized failure modes: Two competing mechanisms. *International Journal for Numerical and Analytical Methods in Geomechanics*, 35(5), pp.586–601.

Nova, R., 1994. Controllability of the incremental response of soil specimens subjected to arbitrary loading programs. *Journal of the Mechanical Behavior of Materials*, 5(2), pp.193–202.

Oreste, P.P., 2003. Analysis of structural interaction in tunnels using the covergence–confinement approach. *Tunnelling and Underground Space Technology*, 18(4), pp.347–363.

Panet, M., 1995. Le calcul des tunnels par la méthode Convergence-Confinement. *Presses des Ponts et Chaussées*.

Panet, M., Bouvard, A., Dardard, B., Dubois, P., Givet, O., Guilloux, A., Launay, J., Piraud, J. and Tournery, H., 2001. *AFTES Recommendations on the Convergence–Confinement Method*. Paris, France: Association Française des Tunnels et de l'Espace Souterrain (AFTES).

Prunier, F., Chomette, B., Brun, M. and Darve, F., 2016. Designing geotechnical structures with a proper stability criterion as a safety factor. *Computers and Geotechnics*, 71, pp.98–114.

Prunier, F., Nicot, F., Darve, F., Laouafa, F. and Lignon, S., 2009. Three-Dimensional Multiscale Bifurcation Analysis of Granular Media. *Journal of Engineering Mechanics*, 135(6), pp.493–509.

Qi, Y., O'Loughlin, C.D. and Bransby, M.F., 2025. Detection and measurement of strain localisations in clay using particle image velocimetry. *International Journal of Physical Modelling in Geotechnics*, pp.1–16.

Vermeer, P.A., Ruse, N. and Marcher, T., 2002. Tunnel heading stability in drained ground. *Felsbau*, 20(6), pp.8–18.

Vlachopoulos, N. and Diederichs, M.S., 2009. Improved longitudinal displacement profiles for convergence confinement analysis of deep tunnels. *Rock mechanics and rock engineering*, 42, pp.131–146.

Zeng, S., Lü, X. and Huang, M., 2019. Discrete element modeling of static liquefaction of shield tunnel face in saturated sand. *Acta Geotechnica*, 14, pp.1643–1652.

Zhang, Z., Xu, W., Nie, W., and Deng, L., 2021. DEM and theoretical analyses of the face stability of shallow shield cross-river tunnels in silty fine sand. *Computers and Geotechnics*, 130, p.103905.